Gazi University Journal of Science
GU J Sci
23(4):475-485 (2010)

GUJS
www.gujs.org

Particulate Sol Route Hydroxyapatite Thin Film-Silk Protein Interface Interactions

Selçuk ÖZCAN[1♠], Muhsin ÇİFTÇİOĞLU[1]

[1]*Izmir Institute of Technology, Department of Chemical Engineering, Urla, Izmir, 35430, Turkey*

Received: 29.03.2010 Revised: 26.04.2010 Accepted: 01.05.2010

ABSTRACT

Hydroxyapatite (HAp) thin film coatings were prepared on bioinert glass slides by a particulate sol method and the effects of intermediate silk fibroin and silk sericin coatings on the HAp film formation and surface topography were examined. The films prepared with smaller crushed particle sols had a higher agglomeration tendency during the drying consolidation step of the thin film formation, and contained agglomerates larger in number and size, which was demonstrated experimentally and in accordance with the DLVO theory. In the thin films prepared on intermediate sericin and fibroin films the number and size of agglomerates were decisively reduced, forming homogeneous films of predominantly primary particles, especially for the larger particle size sols. The regular surface electrostatic potential arrangements of the β-sheet structures of the sericin and fibroin, and of hydroxyapatite crystals, gave rise to the coulombic attraction driven surface energy minimization, enhancing the hydroxyapatite thin film formation process. The positive degree of cooperativity in the hydroxyapatite particle deposition on the silk protein coatings was disrupted by the particle agglomeration tendency.

Key Words: *Hydroxyapatite, Particulate sol, Thin film, Silk sericin, Silk fibroin, Protein adsorption, Agglomeration.*

1. INTRODUCTION

Biocompatible mineral coatings on metallic in vivo hard tissue implants act as local scaffolds for enhanced osteoconduction, providing fast bone apposition and cementless fixation [1]. Hydroxyapatite (HAp), $Ca_{10}(PO_4)_6(OH)_2$, has been experimentally determined to be one of the best implant coating materials for post operative osteogenic cell proliferation and differentiation on the implant surface (osteoinduction) resulting in the growth of the surrounding hard tissue based on the concerted dynamic resorption-precipitation-bone substitution in vivo processes [2,3,4]. Plasma spraying of HAp is the most widely employed industrial method for bioactive calcium phosphate (CaP) coatings. However, there is a general tendency to develop new routes for hydroxyapatite coatings on implant materials due to the fact that the coatings produced by the plasma spray method have a number of disadvantages, namely, inhomogeneous chemical composition and crystallinity, formation of in vivo fast dissolving and unfavorable phases (α-tricalcium phosphate, tetracalcium phosphate, oxyhydroxyapatite, calcium oxide and amorphous

♠Corresponding author, e-mail: selcukozcan@iyte.edu.tr

phases) in the interface, thermal stress and amorphous to crystalline phase transformation stress crackings, and delamination or even detachment of the coating layer [1,4-10]. Sputter coating [10, 11], pulsed laser deposition [12,13], electrophoresis [14-18], electrochemical deposition [16,19], thermal substrate method [20], aerosol-gel method [21], biomimetic formation [22,23], and sol-gel deposition [1,4,24-28] can be listed as alternative CaP film formation techniques. Hydroxyapatite thin film coatings prepared by the sol-gel methods have attracted much attention due to the inherent advantages of being chemically and physically homogeneous and pure, capability of tailoring chemical composition, porosity, pore size and surface roughness, besides the relative simplicity of the method.

Silk and especially silk fibroin have been used for a variety of biomedical applications, ranging from biomedical suture for centuries, to the recently exploited potential uses for controlled release [29] and scaffolds for tissue engineering [30]. The favorable interactions between hydroxyapatite, and silk fibroin and silk sericin in biomimetic nucleation and crystal growth of hydroxyapatite deposits were experimentally observed [31-33]. The aspartate, arginine and glutamate residues are arranged in polar clusters in the β-sheet structure of fibroin, inducing a surface electrostatic potential distribution due to the hydroxyl, carboxyl, and carbonyl groups that have an affinity for calcium ions. This provides local concentrations of Ca^{2+} leading to the nucleation of HAp crystals. HAp is deposited in the form of tiny crystals on fibroin due to the regular surface arrangement of nucleation sites distributed on a molecular scale [31,32]. In the β-sheet structure of sericin, 10% of the carboxyl groups are perpendicular to the plane of the sheet, providing a periodic distribution of electrostatic potential surface sites which induce coulombic affinity for Ca^{2+} ions leading to the HAp nucleation and crystal growth [33].

In this study, hydroxyapatite thin film surfaces were prepared on bioinert glass substrates by a particulate sol route. The conditions for the formation of continuous films were determined. The relation of the particle agglomeration tendency to the particle size was shown experimentally. The effects of intermediate silk fibroin and silk sericin layers on the HAp film formation, particle agglomeration, and surface topography were examined.

2. MATERIALS AND METHODS

2.1. Hydroxyapatite Particulate Sol Preparation and Characterization

A commercially available hydroxyapatite powder (c-HAp; Sigma C 567-500G) was used as received, and after dry ball milling. The grinding was carried out in a 250 ml tungsten-carbide jar with the grinding medium that comprised 30 pieces tungsten-carbide balls of 1 cm in diameter. Each load for milling consisted of 15 gr of c-HAp. The tungsten carbide jar was gyrated for a maximum of 120 minutes at 400 rpm with intermittent 15 min grinding and cooling periods (from this point on the 120 mindry milled powder will be denoted as m-HAp powder; m for dry milled).

The suspensions of HAp powders were prepared in deionized water. Their dispersion was carried out by wet ball milling in 100 ml jars with a grinding medium of zirconia balls (30gr of Ø5mm and 15 gr of Ø3mm) for 2 hours at 200 rpm, followed by ultrasonic treatment (30 kHz) for another 2 hours. Hydropalate 64 (sodium di-isooctylsulfosuccinate; $C_{20}H_{38}O_7S$, MW=422.58) was added as a dispersing agent at various quantities (0 to 3.6% by weight), and the pH was adjusted between 7 and 11 with 0.1 N NH_4OH. The solid contents of the prepared suspensions were between 1.0 and 25% (by weight).

The particle size distribution of the suspensions was determined by laser scattering (Zeta Sizer; Malvern Instruments Ltd. 3000 HSA). The suspensions were diluted in three steps to a solid content of 0.17 g/L for the laser scattering measurements, readjusting the pH values between 7 and 11. The suspensions were ultrasonically treated for an additional 15 minutes while stirring just before the measurements.

The isoelectric points (IEP) of the c-HAp and m-HAp powder suspensions (0.17 g/L) were measured by laser scattering (Zeta Sizer), determining zeta potentials ($Ø_ζ$) as a function of suspension pH between 3.5 to 10. The point of zero charges (PZC) of the suspensions (1.0%) were determined by continuous automatic titration. The initial pH of the suspensions were adjusted to approximately 11.5 by the addition of 1.0 N of NH_4OH. The suspensions were titrated with automatic dispense of 1.0 N HNO_3 with an initial dispense rate of 0.05 mL/s, while near the inflection point the dispense rate decreased to 0.005 mL/s, generating a continuous pH versus added acid volume diagram. During acid dispensing the suspensions were stirred with a magnetic stirrer.

2.2. Thin Film Silk Sericin and Silk Fibroin Preparation and Characterization

The silk sericin solution was prepared by dissolving 4.2 gr of commercial sericin (Silk Biochemical Co. Ltd., ref: 46-3-108) in 48 ml of deionized water.

Silk fibroin solutions were prepared by the subsequent processes of degumming and dissolution of the raw silk (Silk Biochemical Co. Ltd., ref no: biosilk 04056). The degumming was carried out by boiling in 0.05% aqueous Na_2CO_3 solution (2.0 gr of silk in 100 mL) for 30 minutes. The degummed silk was washed with deionized water and dried at ambient conditions. 1.2 gr of the degummed silk was further treated with 20 times of Ajisawa's reagent (24 mL of $CaCl_2$/ethanol/water: 111/92/144 by weight) in a 250 mL Schott bottle by stirring at 78 ºC for 2 hours to obtain a clear solution. Higher concentrations of fibroin were avoided due to the gelation tendency during the following dialysis step. The fibroin solution was dialyzed in cellulose dialysis tubings against deionized water at 4 ºC by frequent change of dialysis water for the removal of $CaCl_2$ and other neutral salts until tested negative for AgCl precipitation by $AgNO_3$ (approximately 3 days). The treated cellulose tubings were rated to retain protein molecules of over 12 kDa. The silk fibroin solution (1-2% w/v) in the dialysis tubings was filtered (Filtrak 389 filter paper) and concentrated to approximately 10% w/v by a rotary vacuum evaporator at 30 ºC, 30 rpm.

The sericin and fibroin film coatings on bioinert glass substrates were prepared by dip coating in the sericin, and fibroin solutions with a retraction rate of 100 mm/min at ambient temperature (25°C), and with 30 minutes of drying at ambient conditions between dippings. Three

layers of sericin, and fibroin films were formed, and held in an oven at 40°C for 2 hours in order to form water insoluble β-sheet structures.

The sericin, and fibroin films were characterized with FTIR spectroscopy (Digilab-Merlin with the 80° V-gold mirror grazing accessory), SEM imaging (Philips XL-30S FEG), and AFM (Digital Instruments MMSPM Nanoscope IV, in the tapping mode).

2.3. Hydroxyapatite Thin Film Preparation and Characterization

The particulate hydroxyapatite sols were stabilized both sterically (by 2.4% w/w hydropalate 64), and electrostatically (pH=9.4-10.0 by 1.00 N NH_4OH). Glass slides as received, and sericin and fibroin coated glass slides were used as substrates. These substrates were dip coated in the HAp sols at 25ºC with a retraction rate of 100 mm/min, in order to prepare thin film coatings of hydroxyapatite. The films were dried for 1 hour at ambient conditions between the coatings (1 to 5 times). Some of the thin films of HAp were heat treated at 560ºC for 30 minutes in order to observe if any significant sintering of HAp particles would take place and the probable effects in the microstructure of the films..

The HAp thin films were characterized with XRD (Philips X-Pert Pro x-ray diffractometer, CuKα λ=1.54187 Å, in the grazing mode with an incidence angle of 1° and a scan rate of 0.10°/min), and SEM imaging. The film thicknesses were measured with surface roughness tester (Mitutoyo SJ-301) in the profile mode, generating a length-depth profile of the film scratched with an 85 shore A hard rubber.

3. RESULTS AND DISCUSSION

As a result of the dry ball milling of the c-HAp powder an abrupt increase in the tapped bulk density was observed. The change was from 0.44 gr/cm^3 of the c-HAp powder to 0.96 gr/cm^3 of the m-HAp powder. The corresponding SEM images are given in Figure 1. The commercial powder consisted of rod like particles of 150-250 nm in length and 50-80 nm in diameter, while the dry milled powder consisted of equiaxed particles of 40-100 nm in diameter.

The optimum pH values for the dispersion of c-HAp and dry milled powder suspensions were determined by the laser scattering measurements, and the results as number mean particle size versus pH, are shown in Figure 2. The pH values for the minimum agglomerate sizes were in between 10.2 for the c-HAp powder and 9.4 for the m-HAp powder (120 minutes dry milled). The pH for the minimum number mean agglomerate size decreased with the increasing dry milling time and for that matter with the increasing particle surface area.

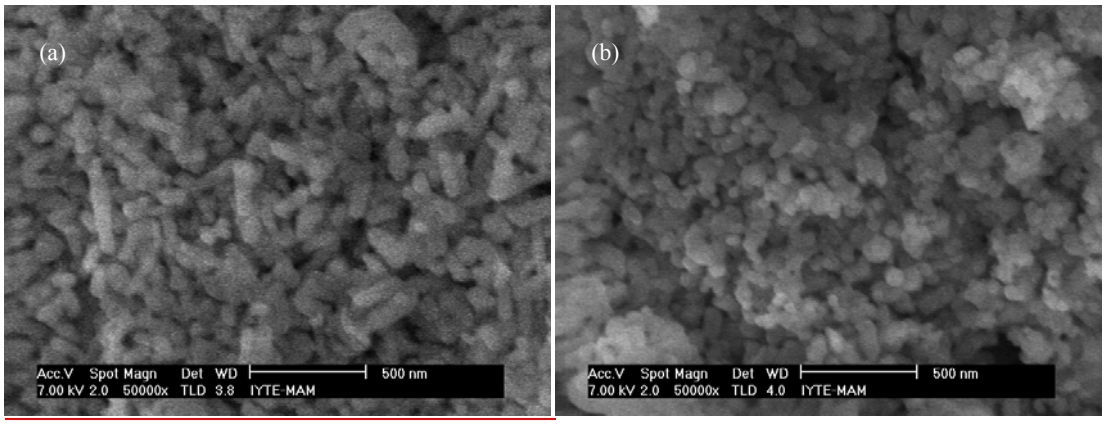

Figure 1. The SEM images of (a) c-HAp powder, (b) m-HAp powder (120 minutes dry milled).

According to the DLVO theory the colloidal suspensions can be electrostatically stabilized by the double ionic layer repulsion [34]. The increasing surface negative charge with the increasing pH was counteracted with a concentration of positive counter ions within the double layer. For the suspension systems of HAp examined, there existed threshold values of the negative surface charge (or of pH), beyond which further increase caused an increase in the double layer counter ion charge at a rate higher than the adsorption rate of surface ion charge (most probably beyond the mono layer surface coverage). This, in turn, gradually lowered the absolute value of the zeta potential ($Ø_\zeta$) at the slip plane, beyond the threshold pH, resulting in the observed minimums in Figure 2.

On the other hand, the increasing surface negative charge with the increasing surface area was counteracted with a concentration of positive counter ions within the double layer, nevertheless, increasing at a rate higher than the increasing surface area. This phenomenon rendered a lower magnitude of negative $Ø_\zeta$ with the increasing surface area (or decreasing particle size), and the absolute value maximums of $Ø_\zeta$ occured at lower pH values, corresponding to the minimums in Figure 2. Direct measurements confirmed this argument, since $Ø_\zeta$(c-HAp, pH=10.2)=-26.3 mV, while $Ø_\zeta$(m-HAp, pH=9.4)=-19.9 mV.

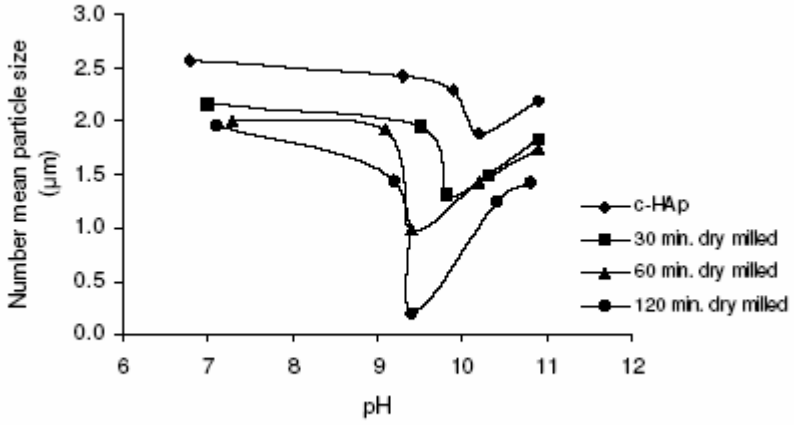

Figure 2. Number mean particle size distributions as a function of pH measured by zeta sizer.

The PZCs of the suspensions were determined as the threshold points at which the surface charges of the HAp particles were reversed (from negative to positive) during the continuous automatic titration indicated by the inflection points in the pH versus added acid volume diagrams. The results showed that the surface charges of the c-HAp and m-HAp powders were neutralized at pH 5.71 and 5.47, respectively, which are, in fact, the PZC values. The IEPs for the c-HAp and the m-HAp powder suspensions were determined to be 5.86 and 5.69, respectively, as the pH values corresponding to $Ø_\zeta=0$. Since the surface is still negatively charged at the IEP, H_3O^+ ion concentration is to be lower compared to the zero surface charge case, and $\zeta=0$ occurs at a higher pH, hence, IEP > PZC for both of the suspensions. The PZC and IEP of the m-HAp powder were lower as compared to the c-HAp powder indicating a higher surface charge due to the higher surface area of the dry milled powder. The charge carried within the slip plane at the IEP was calculated from the difference of the PZC and the IEP, as +0.32 coul/gr HAp for the c-HAp powder, and +0.77 coul/gr HAp for the m-HAp powder. An increase in particle surface area of 23% (from 22 m^2/gr of the c-HAp powder to 27 m^2/gr of the m-HAp powder; estimated geometrically from the SEM images in Fig. 1) brought about a 2.4 times increase in the slip layer charge. The decreasing particle size (or the increasing particle surface area) reduced the double layer repulsive barrier potential, because of the increased screening of the counter-ions within the double layer, hence deteriorated the suspension stability. It also indicated a higher agglomeration tendency of the dry milled powders as compared to c-HAp during thin film formation when particles were forced to compact together by suspension medium evaporation.

The agglomerate sizes for all of the powders rapidly decreased until about 1.2% dispersant (hydropalate 64) was added and higher quantities did not significantly affected the deflocculation.

The HAp coatings were prepared on glass substrates by dip coating as described above. The minimum solid content of the suspensions was determined to be 15% (by weight) for complete surface coverage of the substrates coated with c-HAp; with the same solid content approximately 90% of the substrate surfaces were coated with the m-HAp. The SEM images of the thin film coatings prepared with 15% c-HAp and m-HAp powder suspensions are shown in Figure 3 and Figure 4, respectively. The maximum agglomerate sizes were determined to be 2 μm for the c-HAp coatings, and 5 μm for the m-HAp coatings. The agglomerates of the sizes from 450 nm to 1 μm were most abundant for either type of the coatings. Although the solid content of the m-HAp powder suspension was the same as that for c-HAp, the reason that the substrates coated with the former being slightly short of full surface coverage, was most likely because of the agglomerates larger in size and number, consuming more HAp particles, and depriving the rest of the film of the coating material. The agglomerates larger in number and size in the m-HAp coatings, proved to be an indication of the higher agglomeration tendency, during the drying/particle compaction step of the thin film formation, with increasing surface area, and hence, lower zeta potential of the crushed particles in the suspensions. The thicknesses of the c-HAp, and m-HAp thin films were in the range of 450 nm to 650 nm, and 500 nm to 750 nm, respectively.

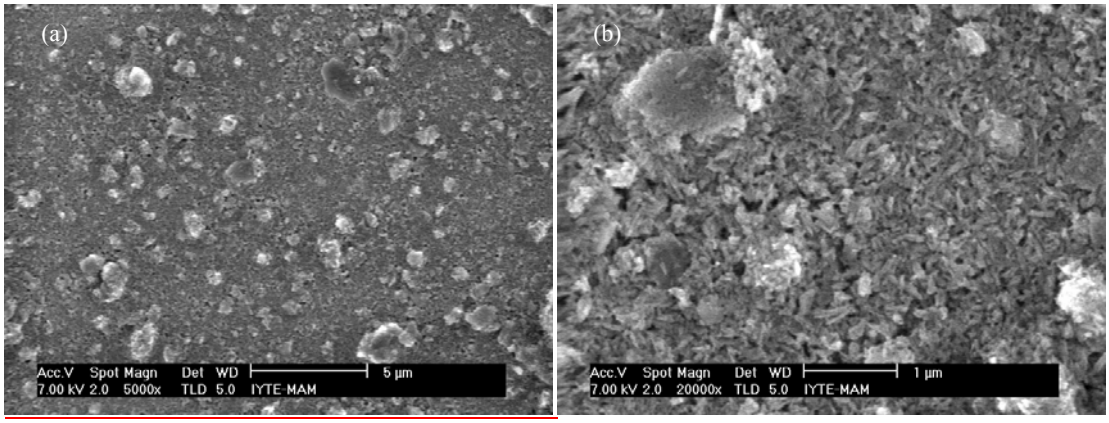

Figure 3. The SEM images of the c-HAp films on the glass substrates prepared by dip coating in 15% solid content suspension at various magnifications (a) 5 000 (b) 20 000x.

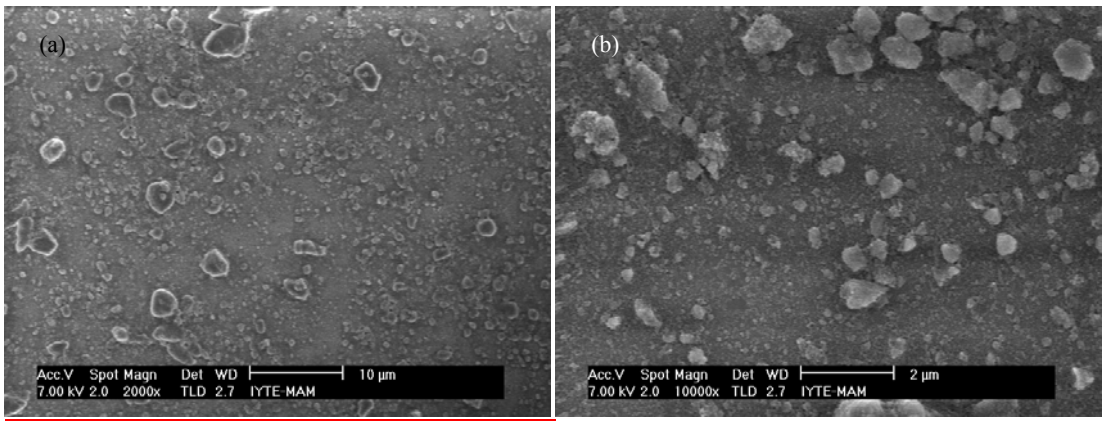

Figure 4. The SEM images of the m-HAp films on the glass substrates prepared by dip coating in 15% solid content suspension at various magnifications (a) 2 000 (b) 10 000x.

The thin film grazing incidence XRD patterns of the c-HAp and m-HAp coatings with and without the heat treatment (at 560°C) are given in Fig. 5. All of the patterns showed purely hydroxyapatite peaks superimposed on the amorphous glass pattern. Heat treatment at that temperature had no detectable effects on the crystallinity of the hydroxyapatite films, and there were not any phase changes, as can be expected. The chemistry of the c-HAp and the m-HAp surfaces were thus taken as identical [35]. However, the relative intensities of the major peaks of the HAp crystal at 2θ values of 31.8º of (211) plane, 32.9º of (300) plane and 32.2º of (112) plane, were higher in the m-HAp films in comparison to the c-HAp films. This most probably pointed out to an oriented crystal structure in the c-HAp films, which might be possible by the alignment of rod like c-HAp crystals (grown in a particular crystal direction during powder production) on the substrate. This particular crystal orientation might have, in turn caused, a decrease in the intensity of scattered radiation from certain crystal planes. In the m-HAp films the crystal orientation should have been random, since m-HAp powder consisted of equiaxed particles which were the crushed forms of the rod shaped grains of c-HAp. Hence, the XRD patterns of the m-HAp films were expected to be identical with that of crystalline HAp powder. As a matter of fact it was reported in the literature that highly oriented polycrystalline thin films can be prepared by sol-gel methods [36,37].

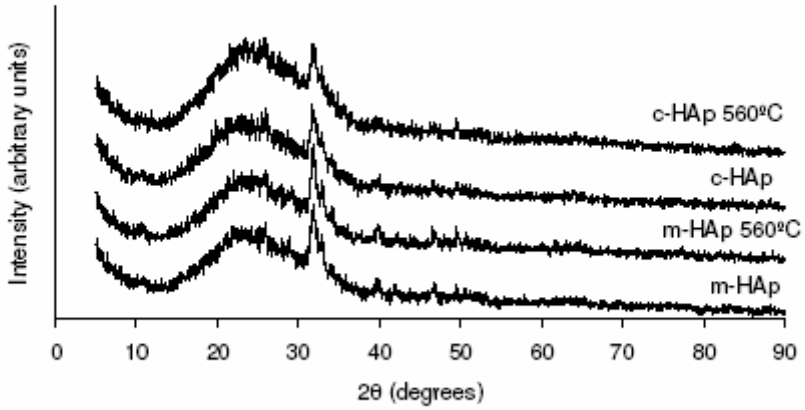

Figure 5. Thin film XRD patterns of c-HAp and m-HAp coatings on glass before and after heat treatment at 560ºC with a grazing incidence angle of 1º.

The AFM images of the sericin film given in Figure 6 actually showed a granular total surface coverage with the average granular size being in the range of 150-250 nm. The thicknesses of the sericin films were determined to be 2 µm on the average. The AFM images of the fibroin film given in Figure 7 again showed a total surface coverage with discernable grains of sizes 100-200 nm. The grains tend to align in straight lines reminiscent of fibrous structures. The thicknesses of the fibroin films were 1.5 µm (less than their sericin counterparts).

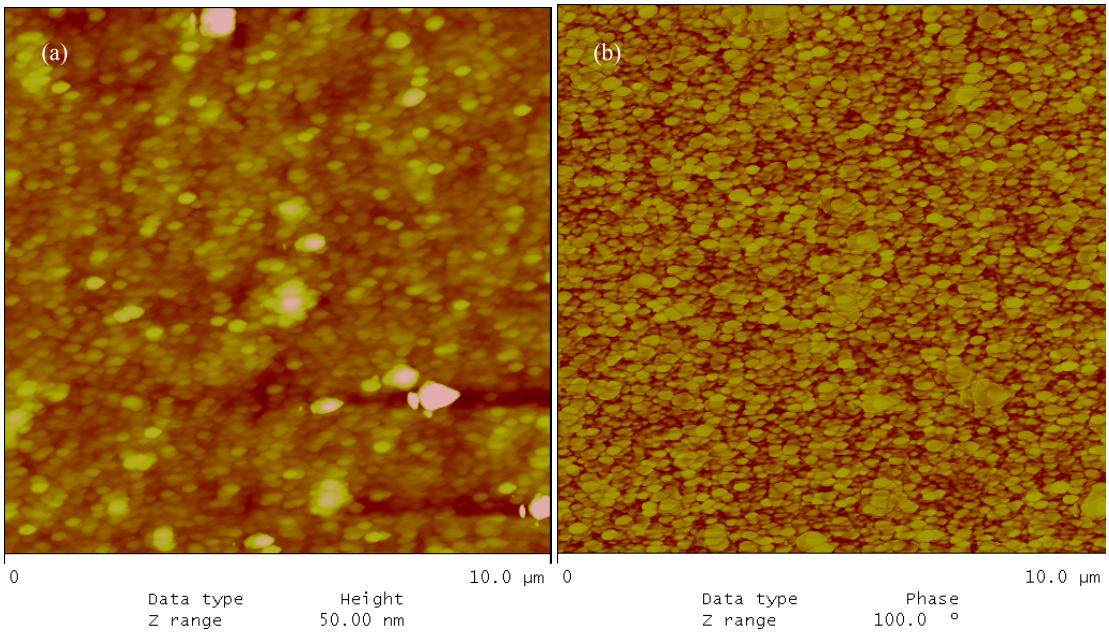

Figure 6. The AFM images of the sericin film on glass substrate (a) 2-dim. topographical and (b) phase images 10x10µm.

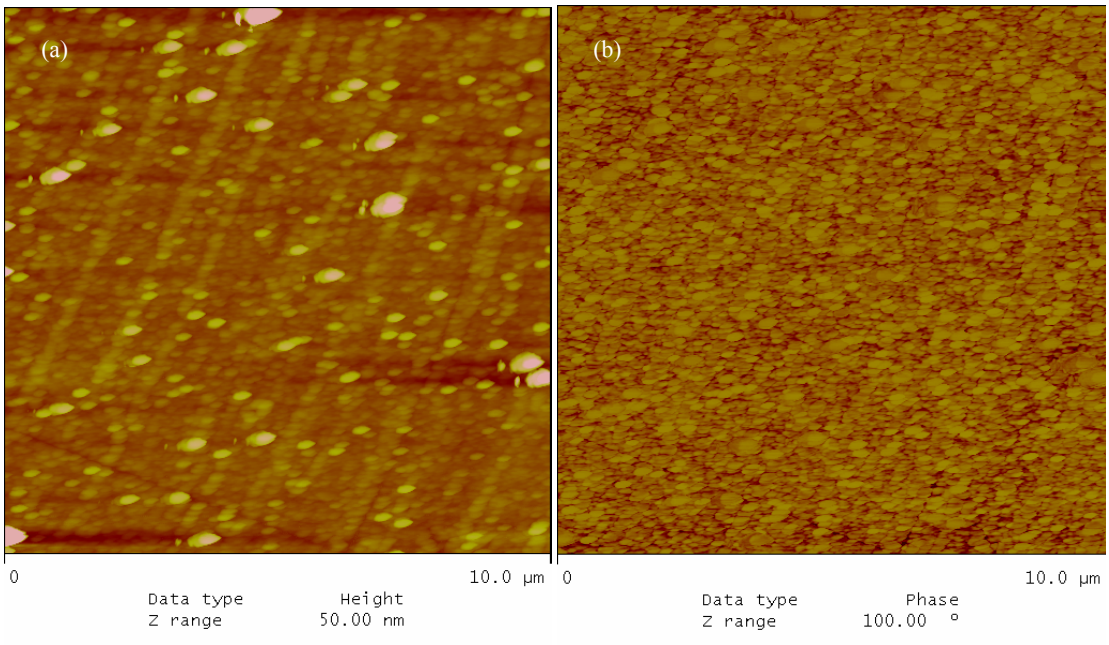

Figure 7. The AFM images of the fibroin film on glass substrates (a) 2-dim. topographical and (b) phase images 10x10µm.

The FTIR spectra of the sericin and fibroin films shown in Figure 8, showed amide I (C=O stretching), and amide II (N-H in-plane bending) vibrations. The amide I νC=O peaks at 1645 cm^{-1} for the fibroin film and at 1640 cm^{-1} for the sericin film and shoulders at 1626 cm^{-1} for both films, and the amide II δN-H peaks at 1535 cm^{-1} and shoulders at 1525 cm^{-1} and 1517 cm^{-1} for both films were attributed to the β-sheet structures of the proteins rather than random coil structures [33,38].

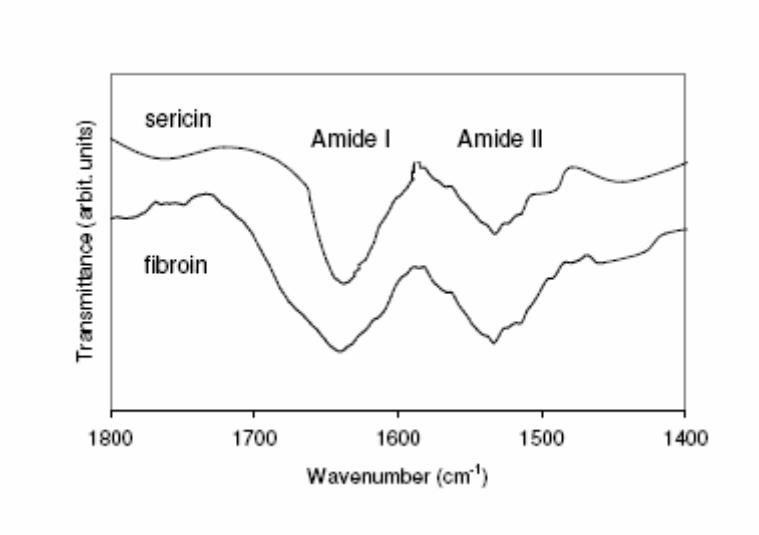

Figure 8. The FTIR spectra of sericin and fibroin films on glass substrates.

These sericin and fibroin coated glasses were used as substrates for the dip coating of 15% solid content c-HAp, and m-HAp particulate sols. The films coated on the glass/sericin substrates were totally transparent, while the films on the glass/fibroin substrates were slightly opacified. The SEM images of the c-HAp films on glass/sericin substrates are shown in Figure 9. The films were decisively more homogeneous as compared to their counterparts coated on glass substrates. The agglomerate sizes were also less than 300 nm explaining the visible light transparency of the films. The surfaces were predominantly covered by primary particles, and the thickness of the HAp layer on top of the sericin layer was measured to be 150-200 nm, indicating a film of 3-4 layers of primary particles compaction.

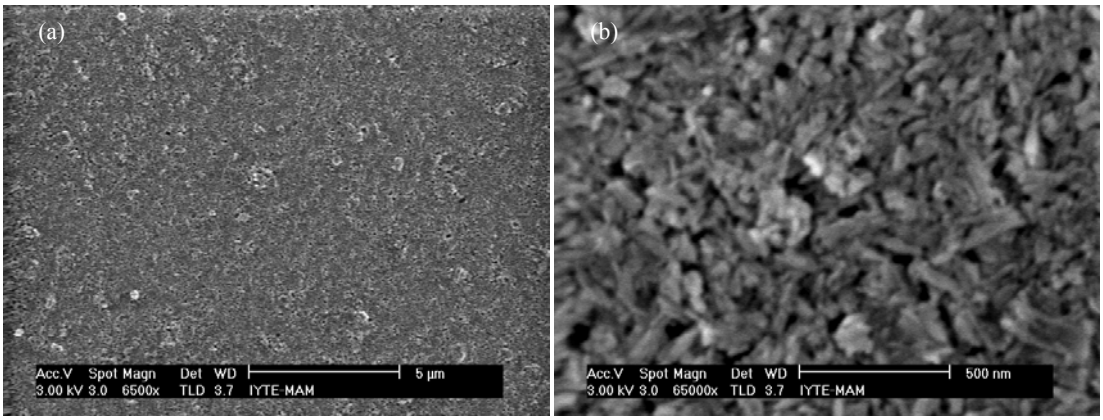

Figure 9. The c-HAp films (with 15% solid content suspension) on glass/sericin substrate at various magnifications

(a) 6 500x (b) 65 000x.

The SEM images of the m-HAp films on glass/sericin substrates are shown in Figure 10. Again the films were decisively more homogeneous as compared to their counterparts coated on glass substrates. However, the surfaces were covered predominantly by agglomerates, evidencing the increased agglomeration tendency of the higher surface area particles. The films were still visible light transparent since the agglomerate sizes were less than 300 nm. The thickness of the HAp layer on top of the sericin layer was measured to be 150-200 nm.

The SEM images of the c-HAp films on glass/fibroin substrates are shown in Figure 11. The films were more homogeneous as compared to their counterparts coated on glass substrates. However, the agglomerate sizes were in the range 400 nm-1 µm, and covered approximately 35% of the surface, partially reflecting light as well as scattering, which explains the slightly opacified appearance of the films. The thickness of the c-HAp layer on top of the fibroin layer was measured to be 150-200 nm. This again corresponds to a film of 3-4 layers of packed primary particles.

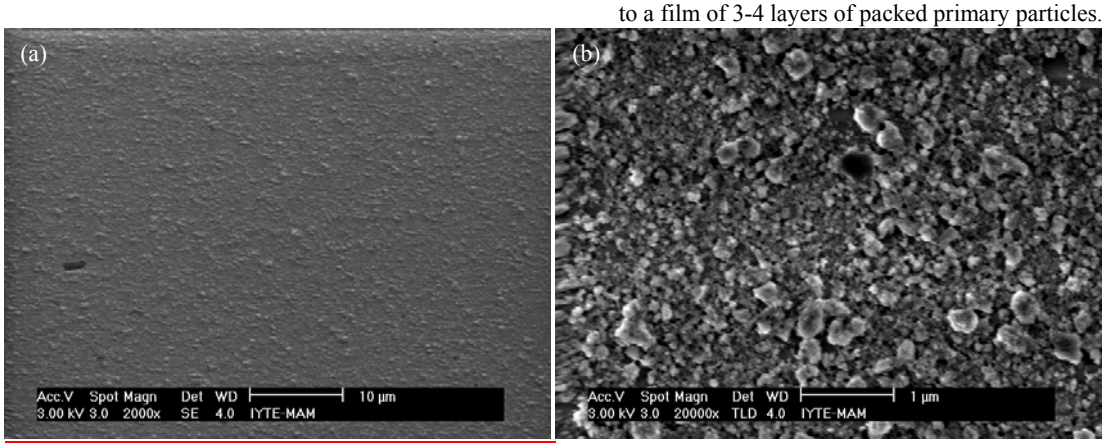

Figure 10. The m-HAp films (with 15% solid content suspension) on glass/sericin substrate at various magnifications

(a) 2 000x (b) 20 000x.

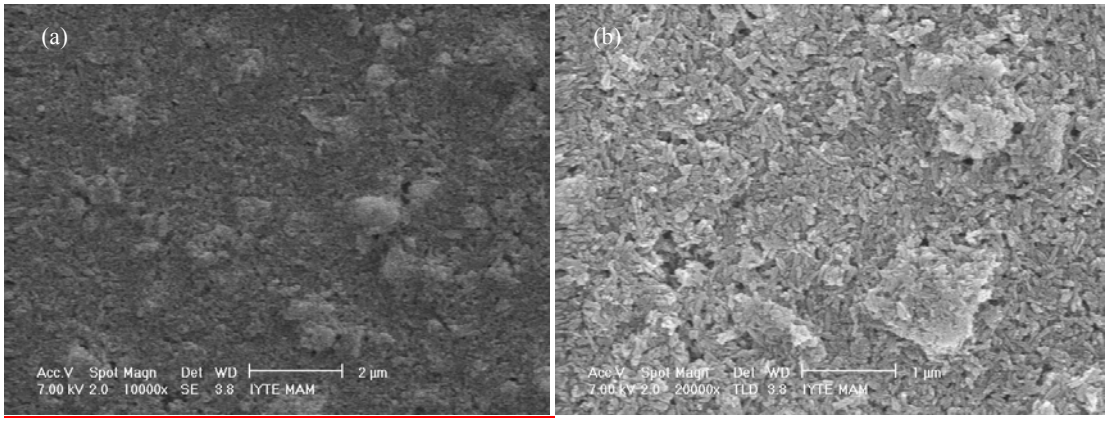

Figure 11. The c-HAp films (with 15% solid content suspension) on glass/fibroin substrates at various magnifications

(a) 10 000x (b) 20 000x.

The SEM images of the m-HAp films on glass/fibroin substrates are shown in Figure 12. Again the films were more homogeneous as compared to their counterparts coated on glass substrates. The maximum agglomerate size was close to 2 μm, and predominantly the agglomerate sizes were less than 500 nm. The films were again slightly opacified. The thickness of the m-HAp layer on top of the fibroin layer was measured to be 250-600 nm.

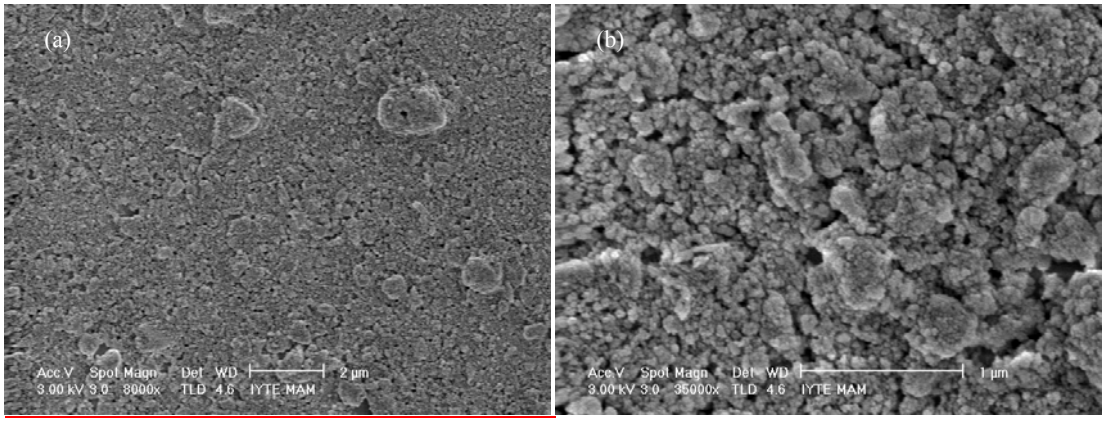

Figure 12. The m-HAp films (with 15% solid content suspension) on glass/fibroin substrates at various magnifications

(a) 8 000x (b) 35 000x.

Apparently the effect of intermediate sericin and fibroin films was the selective deposition of particles of minimal available sizes, predominantly of the primary particles. The affinity of the spatially recurring carboxyl groups ($-COO^-$) in the β-sheet structure of silk proteins, for Ca^{2+} of the hydroxyapatite crystal was reported in the literature; the other possibility that amino groups, $-NH_3^+$ or $=NH_2^+$, to have an affinity for PO_4^{3-} in the hydroxyapatite crystal was considered as a minor effect in comparison to the former because of the polar concentrated arrangement (rather than regular spatial arrangement) of these groups in the β-sheet protein structure [30-33].

The forces in effect for the hydroxyapatite particle deposition on the silk sericin and fibroin films were the same as adsorption phenomenon. By that token the HAp particle deposition during the thin film formation process was most likely regulated by the coulombic interaction between the regularly periodic arrangement of negative electrostatic potential surface sites of sericin and fibroin in the β-sheet structure provided by the $-COO^-$ groups, and the recurring positive electrostatic potential surface strip sites rich in Ca^{2+} on the (100) and (010) faces of hexagonal HAp crystals. On the (001) face of the HAp crystal lattice, 6 oxygen ions that belong to three crystal phosphates create negative potential sites, which may have an coulombic attraction for the polar $-NH_3^+$ groups in the β-sheet structure. The former coulombic interaction probably provided a partially positive degree of cooperativity for the HAp particle deposition on the sericin and fibroin surfaces; together with the latter coulombic interaction the degree of cooperativity might change from partially positive to positive [39]. However, the agglomeration tendency between the HAp particles was a factor that reduced the degree of cooperativity.

The thin coatings of essentially primary particles of HAp, with drastically reduced number and size of agglomerates, and increased homogeneity on the sericin, and the fibroin films were thus resulted from the surface energy minimization of the deposition process driven by coulombic attraction, and probably pointed out to a high degree of positive cooperativity. The agglomeration tendency of the smaller size HAp particles caused the deterioration of the degree of cooperativity, and hence, the surface homogeneity which was visible in the coatings glass/sericin/m-HAp, and especially glass/fibroin/m-HAp, in Fig. 10 and 12, respectively. The coatings with the larger particle size HAp, namely, glass/sericin/c-HAp and glass/fibroin/c-HAp in Figure 9 and 11, respectively, indicated a lower tendency for agglomeration and a more homogeneous film structure which was most probably the result of a higher degree of positive cooperativity in the deposition. Another reason of the phenomenon could be the deposition of c-HAp particles with a certain crystal orientation that would provide a surface with a regular electrostatic potential distribution, as evidenced by the XRD patterns shown in Figure 5.

On the other hand the HAp coatings on sericin were more homogeneous with less agglomerates of smaller sizes in comparison to coatings on fibroin. This might be due to a more pronounced random coil structure with respect to β-sheet structure in the fibroin films, and due to an inherent surface electrostatic potential distribution even in the β-sheet structure of fibroin reducing the degree of positive cooperativity for HAp deposition. The surface electrostatic potential distribution regularities are expected to be delimited by the surface topography, and crystal size, shape and orientation which were factors in determining the HAp particle deposition on the sericin and fibroin surfaces.

The authors showed in an unpublished study that the model protein (bovine serum albumin) adsorption capacity of the c-HAp films formed on the intermediate sericin films increased more than double, in contrast to the HAp films without an intermediate sericin film. In general, silk protein surfaces facilitate the deposition of hydroxyapatite particles grown at a certain crystal orientation, by electrostatic interaction yielding an oriented polycrystalline surface. Such HAp surfaces most probably enhance the adsorption of bone morphogenetic proteins (BMPs) again by electrostatic interaction. This is

the case for the films prepared with c-HAp powder, while the films prepared with its chemically identical crushed form m-HAp powder lack a certain crystal orientation for the electrostatic interaction for protein adsorption.

4. CONCLUSION

In this study it was shown that, formation of a continuous thin film on a substrate by dip coating in the particulate sol required a minimum threshold suspension solid content. For the hydroxyapatite thin film formation on bioinert glass substrates, the threshold solid content of the particulate sols was determined as 15% by weight. During the drying compaction step of the thin film formation, the increasing hydroxyapatite particle agglomeration tendency with decreasing particle size was demonstrated experimentally. The films prepared with smaller particles comprised agglomerates larger in number and size. The favorable interactions between the silk protein coatings and hydroxyapatite particles were observed. The number and size of agglomerates in the c-HAp films (prepared by commercial, higher particle size powder) were decisively reduced on the silk protein layers, forming homogeneous films of predominantly primary particles. This interaction was most probably due to the coulombic attraction driven surface energy minimization for the deposition of HAp particles on the silk sericin and silk fibroin surfaces. The β-sheet structure of the silk proteins provided regular arrangement of negative electrostatic potential surface site distribution due to the $-COO^{-}$ groups, and together with the recurring positive electrostatic potential strips rich in Ca^{2+} on the (100) and (010) faces of HAp crystals, a positive degree of cooperativity enhanced the deposition process. Nevertheless, the agglomeration tendency of the smaller HAp particles adversely affected the degree of cooperativity as in the case of the m-HAp coatings (prepared by dry milled powder). Therefore, such structures may prove effective in cytokine and growth factor (BMPs) adsorption on the implant surfaces for accelerated peri-implant or fracture healing (BMPs can be loaded prior to implantation, or the coated implant surface will adsorp the growth factors and cytokines in vivo, followed by the migration and the attachment of the pluripotent stem cells).

REFERENCES

[1] Daculsi, G., Laboux, O., Le Geros, R., "Outcome and perspectives in bioactive coatings: what's new, what's coming", ITBM-RBM, 23: 317-325 (2002).

[2] Albrektsson, T., Johansson, C., "Osteoinduction, osteoconduction and osseointegration, ***Eur. Spine Jour.***, 10 (Supp.2):S96-101 (2001).

[3] Lind, M., Overgaard, S., Bunger, C., Soballe, K., "Improved bone anchorage of hydroxyapatite coated implants compared with tricalcium phosphate coated implants in trabecular bones in dogs", ***Biomaterials***, 20: 803-808 (1999).

[4] Best, S.M., Porter, E.A., Thian, E.S., Huang, J., "Bioceramics: past, present and for the future", ***J. Eur. Ceram. Soc.***, 28:1319-1327 (2008).

[5] Heimann, R.B., "Thermal spraying of biomaterials", ***Surface & Coatings Technology***, 201: 2012-2019 (2006).

[6] Radin, S.R., Ducheyne, J., "Plasma spraying induced changes of calcium phosphate ceramic characteristics and the effect on in vitro stability", J. ***Mater. Sci. Mater Med.***, 3: 33-42 (1992).

[7] Cirilli, F., Kaciulis, S., Mattongno, G., Righini, G., Ferrari, F., Montenero, A., "Surface analysis of biocompatible hydroxyapatite coatings on titanium", in: Olefjord J, Nyborg L, Briggs D, editors. Proc. ECASIA 97, 7th European Conference on Applications of Surface and Interface Analysis, Chichester, ***John Wiley and Sons***, 151-154 (1997).

[8] Gross, K.A., Gross, V., Berndt, C.C., "Thermal analysis of amorphous phases in hydroxyapatite coatings", ***J. Am. Ceram. Soc.***, 81: 106-112 (1998).

[9] Gross, K.A., Berndt, C.C., "Thermal processing of hydroxyapatite for coating production", ***J. Biomed. Mater. Res.***, 39: 580-587 (1998).

[10] Massaro, C., Baker, M.A., Cosentino, F., Ramires, P.A., Klose, S., Milella, E., "Surface and biological evaluation of hydroxyapatite-based coatings on titanium deposited by different techniques", ***J. Biomed. Mater. Res. (Appl. Biomater.)***, 58: 651-657 (2001).

[11] Torrisi, L., Foti, G., "Ion sputtering of hydroxyapatite", ***Appl. Phys. Lett.***, 62: 237-239 (1993).

[12] Gyorgy, E., Toricelli, P., Socol, G., Iliescu, M., Mayer, I., Mihailescu, I.N., Bigi, A., Werckman, J., "Biocompatible Mn doped carbonated hydroxyapatite thin film grown by pulsed laser deposition", ***J. Biomed. Mater. Res. Part A***, 71A: 353-358 (2004).

[13] Cotell, C.M., "Pulsed laser deposition and processing of biocompatible hydroxyapatite thin films", ***Appl. Surf. Sci.***, 69: 140-148 (1993).

[14] Wei, M., Ruys, A.J., Milthorpe, B.K., Sorrell, C.C., "Solution ripening of hydroxyapatite nanoparticles: effects on electrophoretic deposition", ***J. Biomed. Mater. Res.***, 45: 11-19 (1999).

[15] Ducheyne, P., Radin, S., Heughebaert, M., Heughebaert, J.C., "Calcium phosphate ceramic coatings on porous titanium: effect of structure and composition on electrophoretic deposition, vacuum sintering and in vitro dissolution", ***Biomaterials***, 11: 244-254 (1990).

[16] Raja, K.S., Misra, M., Paramguru, K., "Deposition of calcium phosphate coating on nanotubular anodized titanium", ***Mater. Lett.***, 59: 2137-2141 (2005).

[17] Zhitomirsky, I., "Electrophoretic hydroxyapatite coatings and fibers", ***Mater. Lett.***, 42: 262-271 (2000).

[18] Albayrak, O., El-Atwani, O., Altintas, S., "Hydroxyapatite coatings on titanium substrate by electrophoretic deposition method: effects of titanium dioxide inner layer on adhesion strength and hydroxyapatite decomposition", ***Surface Coatings Technology***, 202: 2482-2487 (2008).

[19] Ban, S., Maruno, S., "Hydrothermal-electrochemical deposition of hydroxyapatite", ***J. Biomed. Mater. Res.***, 42:387-395 (1998).

[20] Kuroda, K., Ichino, R., Okido, M., Takai, O., "Hydroxyapatite coating on titanium by thermal substrate method in aqueous solution", ***J. Biomed. Mater. Res.***, 59: 390-397 (2002).

[21] Manso-Silvan, M., Langlet, M., Jimenez, J., Fernadez, M., Martinez-Duart, J.M., "Calcium phosphate coating prepared by aerosol-gel", ***J. Eur. Ceram. Soc.***, 23: 234-246 (2003).

[22] Varma, H.K., Yokogawa, Y., Espinosa, F.F., Kawamoto, Y., Nishizawa, K., Nagata, F., Kameyama, T., "Porous calcium phosphate coating over phosphorylated chitosan film by a biomimetic method", ***Biomaterials***, 20: 879-884 (1999).

[23] Liu, D.M., Yanh, Q., Troczynski, T., "Sol-gel hydroxyapatite coatings on stainless steel substrates", ***Biomaterials***, 23: 691-698 (2002).

[24] Cavalli, M., Gnappi, G., Montenero, A., Bersani, D., Lottici, P.P., Kaciulis, S., Mattogno, G., "Hydroxy and fluorapatite films on Ti alloy substrates: sol-gel preparation and characterization", ***J. Mater. Sci.***, 36: 3253-3260 (2001).

[25] Gan, L., Pilliar, R., "Calcium phosphate sol-gel derived thin films on porous-surfaced implants for enhanced osteoconductivity, Part I: synthesis and characterization", ***Biomaterials***, 25: 5303-5312 (2004).

[26] Gan, L., Wang, J., Pilliar, R.M., "Evaluating interface strength of calcium phosphate sol-gel derived thin films to Ti6Al4V substrates", ***Biomaterials***, 26: 189-196 (2005).

[27] Ferraz, M.P., Monteiro, F.J., Manuel, C.M., "Hydroxyapatite nanoparticles: a review of preparation methodologies", ***J. Appl. Biomater. Biomech.***, 2: 74-80 (2004).

[28] Kim, H.W., Knowles, C.J., Salih, V., Kim, H.E., "Hydroxyapatite and fluor-hydroxyapatite layered film on titanium processed by a sol-gel route for hard tissue implants", ***J. Biomed. Mater. Res. (Appl. Biomater.)***, 71B: 66-76 (2004).

[29] Bayraktar, O., Malay, O., Ozgarip, Y., Batigun, A., "Silk fibroin as a novel coating material for controlled release of theophylline", ***Eur. J. Pharmaceutics and Biopharmaceutics***, 60: 373-381 (2005).

[30] Altman, G.H., Diaz, F., Jakuba, J., Calabro, T., Horan, R.L., Chen, J., Lu, H., Richmond, J. Kaplan D.L., "Silk-based biomaterials", ***Biomaterials***, 24: 401-416 (2003).

[31] Kong, X.D., Cui, F., Wang, X.M., Zhang, M., Zhang, W., "Silk fibroin regulated mineralization of hydroxyapatite nanocrystals", ***J Crystal Growth***, 270: 197-202 (2004).

[32] Kong, X.D., Sun, X., Cui, F., Ma, C., "Effect of solute concentration on fibroin regulated biomineralization of calcium phosphate", ***Mater. Sci. Eng.***, C 26: 639-643 (2006).

[33] Takeuchi, A., Othsuki, C., Miyazaki, T., Kamitakahara, M., Ogata, S.M., Yamazaki, M., Furutani, Y., Kinoshita, H., Tanihara, M., "Heterogeneous nucleation of hydroxyapatite on protein: structural effect of silk sericin", ***J. R. Soc. Interface***, 2: 373-378 (2005).

[34] Brinker, C.J., Scherer, G.W., "Sol-gel Science the physics and chemistry of sol-gel processing", San Diego, ***Academic Press Inc.,*** 235-301 (1990).

[35] Dos Santos, E.A., Farina, M., Soares, G.A., Anselme, K., "Surface energy of hydroxyapatite and β-tricalcium phosphate ceramics driving serum protein adsorption and osteoblast adhesion", ***J. Mater. Sci: Mater. Med.***, 19: 2307-2316 (2008).

[36] Hwang, K.S., Kim, B.H., "Preparation of highly oriented $LaNiO_3$ thin films by spin-coating technique", ***Journal of Sol-Gel Science and Technology***, 14: 203-207 (1999).

[37] Chen, Y.C., Sun, Y.M., Lin, C.P., Gan, J.Y., "Enhanced a-axis oriented crystal growth of Nd substituted bismuth titanate thin films with layer by layer crystallization", ***Journal of Crystal Growth***, 268(1-2): 210-214 (2004).

[38] Hofmann, S., Wong, Po Foo, C.T., Rossetti, F., Textor, M., Vunjak-Novakovic, G., Kaplan D.L., Merkle, H.P., Meinel, L., "Silk fibroin as an organic polymer for controlled drug delivery", ***J. Controlled Release***, 111: 219-227 (2006).

[39] Luo, Q., Andrade, J.D., "Cooperative adsorption of proteins on hydroxyapatite", ***J. Colloid and Interface Sci.***, 200: 104-113 (1998).